# Joint registration of attenuation and activity images in gated TOF-PET

Ahmadreza Rezaei, Johan Nuyts

***Abstract*— To date, attenuation correction of gated PET emission data remains a challenge. Joint activity and attenuation estimation methods may contribute to solving this challenge. In this work, we demonstrate a framework in which the gated PET activity and attenuation images are jointly reconstructed and then registered to a reference frame by a joint registration approach. The method is studied and compared to common approaches by means of 2D and 3D simulations.**

## I. Introduction

In gated PET studies, the emission data are collected and organized in different frames corresponding to different phases of the cyclic cardiac or respiratory motion. It is common to reconstruct the gated PET data separately and in an additional step, register each of the frame reconstructions to a reference frame to obtain a motion-free tracer distribution as a sum of all registered frames [1], [2]. Correcting the gated PET data for the corresponding attenuation of the frame is often the most problematic part. One approach is to use the attenuation factors obtained from a cardiac/respiratory gated CT scan. However, this approach tends to be cumbersome and leads to an increase in radiation dose unless ultra-low dose protocols are applied [3]. Moreover, there can still be misalignment between the CT and PET frames, due to patient motion and deviations in the cyclic motion. Therefore, it would be preferable to acquire a single CT-scan, and register that scan non-rigidly to each of the PET-frames, such that each PET frame can be corrected with a well aligned attenuation map. However, such an accurate delineation is difficult to obtain.

Recent studies on joint estimation of the activity image and the attenuation image [4], [5] or the attenuation sinogram [6]–[9] from time-of-flight (TOF) PET emission data, demonstrate that stable reconstructions of tracer distributions can be obtained independently of previously obtained anatomical images. The guaranteed alignment produced by the joint estimation methods provides a powerful tool, mitigating the problem of incorrect attenuation correction of the PET emission data in 3D and 4D PET studies. Furthermore, the availability of a well aligned pair of activity and attenuation images for each frame may help in between-frame registrations, because both the attenuation and the activity must comply with a single deformation field.

## II. Methods

The main focus of this paper is to study the accuracy in obtaining between-frame (between each gated frame and the reference frame) deformation fields. We study the deformation field accuracy after the gated PET emission data have been corrected for attenuation by attenuation correction techniques most commonly in use. While attenuation correction of the emission data is ignored in some studies, some use an average attenuation or try to deform an initial attenuation with a prior model of the expected between-frame motion. In the latter approach, alignment is never guaranteed and hence we will study the registration results when attenuation correction is done by means of a misaligned attenuation image. These two methods, i.e. (1) ignoring attenuation and (2) the use of a misaligned attenuation map, are then compared to activity registrations and joint registrations of aligned activity and attenuation images which were reconstructed with joint maximum likelihood estimation.

We investigate the effect of the attenuation correction methods by the registration errors they produce. The diffeomorphic implementation of the well known Demons registration algorithm [10] provided by the Insight Toolkit [11] is used to register the reconstructed images to the reference frame. The registration error ($err$) is defined as the difference between the true activity of the reference frame and the registered true activity of the moving frame (1) when the estimated deformation field is applied to it. However, to account for resolution differences between the reference and the moving frames, the deformation and its inverse are applied to the reference frame prior to computing the registration error. The registration error is computed as:

$$err = \frac{\sum_j \|\boldsymbol{D} \circ \boldsymbol{D^{-1}} \circ Act_j^R - \boldsymbol{D} \circ Act_j^M\|}{\sum_j \|Act_j^R - Act_j^M\|} \qquad (1)$$

where, $Act^R$ and $Act^M$ are the true activity of the reference and moving frames, respectively. $\boldsymbol{D}$ is a 3-element vector representing the displacement for each voxel, $\boldsymbol{D^{-1}}$ is its inverse and $j$ is the voxel index.

## III. Experiment Design

The simulation specifications were adjusted according to the Siemens Biograph scanner specifications. The 2D TOF-PET emission data consist of 200 radial bins of 0.4 cm width, 168 projection angles over 180 deg, and 13 TOF-bins of 312 ps width with an effective TOF resolution of 580 ps. An oversampling of 3 was also used during simulations to account for slight mismatch (between projector and simulations), and the reconstructed images had 200 $\times$ 200 pixels of 0.21 cm width, respectively. The 3D TOF-PET data are organized as 5D sinograms, consisting of 200 radial bins, 168 azimuthal

Nuclear Medicine, K.U.Leuven, B-3000 Leuven, Belgium. This research is supported by a research grant (GOA) from K.U.Leuven and by Siemens Healthcare, Anderlecht, Belgium.

angles, 9 co-polar angles, 109 planes, and 13 TOF-bins. The images are reconstructed in a 200 $\times$ 200 $\times$ 109 volume grid with a voxel width of 0.4 cm and 0.2 cm in the transaxial and axial directions, respectively.

A multi-resolution scheme of the diffeomorphic Demons algorithm was used to register the reconstructions in the 2D and 3D simulations. The 2D images were considered registered after a total of 100 iterations (40 and 60 iterations in the coarse and fine resolutions, respectively), and the 3D images were considered registered after a total of 180 iterations (30, 60 and 90 iterations in 3 resolution levels).

### A. 2D Thorax Phantom

A 2D thorax phantom was deformed with a rigid transform followed by a non-rigid transform to create two different frames to be registered in a noise-less simulation. The two frames differ by an increase of the size of the lungs, decrease in the heart size, and a small rotation of 0.1 rad (rotated around the center of the image) of the activity and attenuation phantoms. In addition, noisy TOF-PET emission data were simulated for both frames, the reconstructions of each frame were then registered for a simulation in the presence of noise. Figure 1 shows the activity and attenuation images of the two different frames used in the 2D phantom studies together with the differences between the two frames.

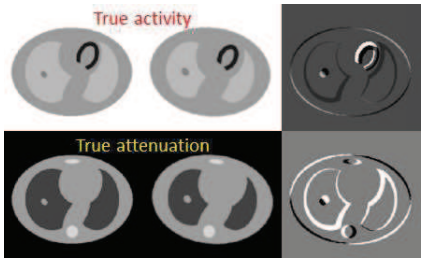


Fig. 1. True activity (top) and attenuation (bottom) images of two different frames (left and center), together with the differences between the activity and attenuation images of the two frames (right).

*1) Joint Registration Simulation:* We use a single displacement field in this study to estimate the displacement between the activity and attenuation images of the two frames. The estimated displacement field was updated in an interleaved manner from activity and attenuation images to avoid the problem of balancing the contributions of two images with different units. The registration results are then compared to the result obtained by registering the activity images only.

*2) Multiple Noise Realization:* The activity and attenuation images of each frame are projected to create TOF-PET emission data and then corrupted with Poisson noise. Activity and attenuation images are then reconstructed from the TOF-PET data using the MLAA (maximum likelihood activity and attenuation estimation) algorithm and jointly registered using a single deformation field. We assumed that knowledge of the total activity counts is available, and the reconstructions were scaled accordingly to overcome the scale/constant problem in MLAA. In addition, for both frames, activity images were reconstructed from the emission sinogram with MLEM (1) without attenuation correction and (2) with attenuation correction, using the attenuation of the first frame.

Using the metric of (1), registration errors are computed for four possible approaches to attenuation correction and displacement field estimation of the moving frame reconstructions to the reconstruction of the reference frame;

- Method I, registration of MLEM activity reconstructions without attenuation correction.
- Method II, registration of MLEM activity reconstructions with a single attenuation image: both frames were reconstructed with the attenuation image of the reference frame (and hence the moving frame suffers from attenuation misalignment).
- Method III, registration of MLAA activity reconstructions.
- Method IV, joint registration of MLAA activity and attenuation reconstructions.

All MLEM and MLAA reconstructions are after 3 iterations of 42 subsets. In MLAA, the attenuation image was updated 5 times for each update of the activity image. We used 100 different noise realizations for the study. The noisy TOF sinograms had an average maximum count of 10.7, and the maximum count in the corresponding non-TOF sinogram was 30.6.

### B. 3D Breathing XCAT Phantom

Two different frames (from a total of 8 frames) in the breathing cycles of the XCAT phantom are projected to create the 3D TOF-PET data. The four attenuation correction and registration strategies are compared to one another after Poisson noise was added to the frame measurements and MLEM and MLAA reconstructions were made accordingly. We used 25 different noise realizations for the study and the emission counts were adjusted to the counts of a typical 10 and 20 minute patient scan injected with the $^{18}$F-FDG radiotracer. The noisy TOF sinograms had an average maximum count of 2.7, and the maximum count in the corresponding non-TOF sinogram was 7.1 for the 10 minute patient scans.

## IV. Results

### A. 2D Thorax Phantom

*1) Joint Registration Simulation:* Figure 2 shows the registration results of between-frame activity registration together with the results of joint activity and attenuation registration of the two frames.

*2) Multiple Noise Realization:* Figure 3 shows the resulting activity and attenuation reconstructions of MLEM and MLAA for each frame after Poisson noise was added to the projection measurements. Using the deformation fields obtained from activity registrations and the one obtained from joint registration of activity and attenuation, the true phantoms were transformed to give an estimate of the registration error. The average absolute registration error images are shown in figure 4, which demonstrates the effectiveness of joint registration of noisy activity and attenuation reconstructions.

Table I shows the average registration errors of the four discussed methods. The registration errors are computed for

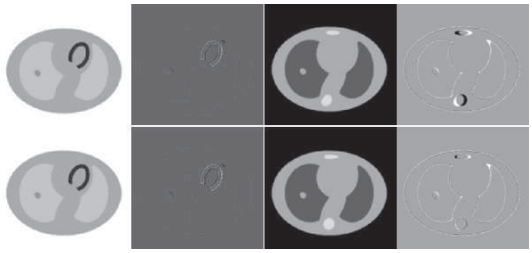

Fig. 2. Activity (top) and joint activity and attenuation (bottom) registration results after applying the deformation to the activity (column 1) and attenuation (column 3) images together with the difference from the true phantoms of the reference frame (columns 2 and 4).

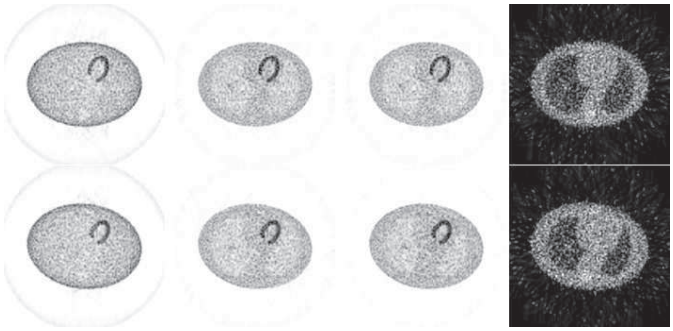

Fig. 3. MLEM activity reconstruction of the TOF-PET emission data without correction for attenuation (column 1), with mismatched attenuation correction (column 2) and MLAA reconstructions of activity (column 3) and attenuation (column 4) of the reference (top) and moving (bottom) frames.

the entire support (SUP) of the activity image, a region-of-interest (ROI) around the tumor (ROI-1) located in the lung and a region-of-interest around the heart (ROI-2). In this simple 2D experiment, it is interesting to see that in all cases the registration error of MLEM activity reconstructions with a misaligned attenuation image is higher than the registration error of MLEM activity reconstructions not corrected for attenuation. We see that the joint registration approach tends to produce the least amount of error compared to all the other approaches. The smallest ROI registration errors were obtained only in methods which used the MLAA aligned attenuation reconstructions. However, the registration errors of ROI-2 did not differ as much as the registration errors of SUP and ROI-1. This is mainly due to the heart activity being reconstructed with a high contrast in all the reconstruction methods (figure 3). The Demons algorithm minimizes the sum of squared differences [10] between the two images, and is therefore most sensitive to registration errors near the heart.

TABLE I

REGISTRATION ERRORS OF THE FOUR ATTENUATION CORRECTION AND REGISTRATION METHODS FOR THE 2D AND 3D STUDIES.

| Method | | I | II | III | IV |
|---|---|---|---|---|---|
| 2D | SUP (%) | 41.9 | 47.1 | 33.1 | 27.0 |
| | ROI-1 (%) | 75.4 | 75.8 | 48.3 | 45.5 |
| | ROI-2 (%) | 19.4 | 20.8 | 20.6 | 19.3 |
| 3D | SUP-10 (%) | 30.6 | 42.9 | 29.9 | 28.9 |
| | SUP-20 (%) | 29.2 | 42.3 | 26.6 | 25.6 |

Fig. 4. Absolute registration error images after the 2D thorax phantoms were deformed by the estimated displacement field. The error images are averaged over 100 noise realizations and correspond to methods I, II, III and IV from left to right.

### B. 3D Breathing XCAT Phantom

Table I also shows the average registration errors of the four methods discussed for the more realistic breathing XCAT phantom. The registration errors are computed within the support of the 3D phantom for the 10 minute scan (SUP-10) as well as the 20 minute scan (SUP-20). As before, we observe that the smallest registration error is obtained when the MLAA reconstructed attenuation images are used to estimate the between-frame displacement field (method IV). We observe that all the registration methods benefit from an increase of the patient scan time, however methods III and IV seem to benefit the most.

## V. CONCLUSION

Attenuation correction of emission data has long been an issue in 4D gated PET studies. We believe that joint activity and attenuation estimation methods may be helpful for solving this longstanding problem. In our approach, the activity and attenuation images of different frames were reconstructed separately using the MLAA algorithm. The activity and attenuation reconstructions of each frame were then jointly registered to activity and attenuation reconstructions of a reference frame, respectively. Our 2D and 3D simulations show that this approach produces the least amount of between-frame registration error among other possible approaches.

## VI. ACKNOWLEDGEMENTS

The authors would like to thank Michel Defrise and Annemie Ribbens for helpful discussions.

## REFERENCES

[1] M Dawood, F Buther, X Jiang, KP Schafers, “Respiratory Motion Correction in 3-D PET Data With Advanced Optical Flow Algorithms” *IEEE Trans Med Imaging*, 2008, 27(8):1164-1175.

[2] SJ McQuaid, T Lambrou, BF Hutton, “A novel method for incorporating respiratory-matched attenuation correction in the motion correction of cardiac PET/CT studies”, *Phys Med Biol*, 2011, 56(10):2903-2915.

[3] T Xia, AM Alessio, B De Man, R Manjeshwar, E Asma, PE Kinahan, “Ultra-low dose CT attenuation correction for PET/CT”, 2012, *Phys Med Biol*, 57:309-328.

[4] A Rezaei, M Defrise, G Bal, C michel, M Conti, C Watson, J Nuyts, “Simultaneous Reconstruction of Activity and Attenuation in Time-of-Flight PET”, Dec 2012, *IEEE Trans Med Imag*, pp. 2224-33.

[5] M Defrise, A Rezaei, J Nuyts, “Time-of-Flight PET data determine the attenuation sinogram up to a constant”, 2012, *Phys Med Biol*, pp. 885-899.

[6] J Nuyts, A Rezaei, M Defrise, “ML-reconstruction for TOF-PET with simultaneous estimation of the attenuation factors”, Oct 2012. *IEEE Nucl Sci Symp Conf Record*.

[7] M Defrise, A Rezaei, J Nuyts, “Simultaneous reconstruction of attenuation and activity in TOF-PET: analysis of the convergence of the MLACF algorithm”, Jun 2013. *Fully3D Imag Recon*.

[8] H Li, G El Fakhri, Q Li, “Direct MAP Estimation of Attenuation Sinogram using TOF PET Data and Anatomical Information”, Jun 2013. *Fully3D Imag Recon*.

[9] VY Panin, M Defrise, J Nuyts, A Rezaei, ME Casey, “Reconstruction of Uniform Sensitivity Emission Image with Partially Known Axial Attenuation Information in PET-CT Scanners”, Oct 2012. *IEEE Nucl Sci Symp Conf Record*.

[10] T Vercauteren, X Pennec, A Perchant, N Ayache, “Diffeomorphic demons: efficient non-parametric image registration”, *Neuroimage*, Mar 2009, 45:61-72

[11] TS Yoo, *et al.*, “Engineering and Algorithm Design for an Image Processing API: A Technical Report on ITK - The Insight Toolkit”, *Stud Health Technol Inform*, 2002, 85:586-592